Environmental Modelling and Software 107 (2018) 141–147

Contents lists available at ScienceDirect

Environmental Modelling & Software

journal homepage: www.elsevier.com/locate/envsoft

Optimisation of flow resistance and turbulent mixing over bed forms

A. Arfaie[a], A.D. Burns[a,*], R.M. Dorrell[b], D.B. Ingham[c], J.T. Eggenhuisen[d], W.D. McCaffrey[e]

[a] School of Chemical and Process Engineering, University of Leeds, Leeds LS2 9JT, UK
[b] Institute of Energy and Environment, University of Hull, Hull, HU6 7RX, UK
[c] Department of Mechanical Engineering, University of Sheffield, Sheffield, S10 2TN, UK
[d] Department of Earth Sciences, Utrecht University, PO Box 80021, 3508 TA Utrecht, Netherlands
[e] School of Earth and Environment, University of Leeds, Leeds LS2 9JT, UK

ARTICLE INFO

Keywords:
Turbulent flow
Roughness
CFD
Bed forms

ABSTRACT

Previous work on the interplay between turbulent mixing and flow resistance for flows over periodic rib roughness elements is extended to consider the flow over idealized shapes representative of naturally occurring sedimentary bed forms. The primary motivation is to understand how bed form roughness affects the carrying capacity of sediment-bearing flows in environmental fluid dynamics applications, and in engineering applications involving the transport of particulate matter in pipelines. For all bed form shapes considered, it is found that flow resistance and turbulent mixing are strongly correlated, with maximum resistance coinciding with maximum mixing, as was previously found for the special case of rectangular roughness elements. Furthermore, it is found that the relation between flow resistance to eddy viscosity collapses to a single monotonically increasing linear function for all bed form shapes considered, indicating that the mixing characteristics of the flows are independent of the detailed morphology of individual roughness elements.

1. Introduction

Many industrial and environmental flows are subject to diminished or enhanced turbulence, and flow resistance due to presence of rough surfaces. In heat transfer applications, rib roughened surfaces are employed to enhance heat transfer characteristics in heat exchanger design (Webb and Eckert, 1972). Experimental and numerical studies have been performed to investigate the enhancement of heat transfer by the presence of roughness elements of a wide range of shapes (Moon et al., 2014; Orlandi et al., 2016). Furthermore, analytical and numerical optimisation studies have been performed in order to search for roughness shapes which optimise both heat transfer and friction loss performances (Kim and Kim, 2006).

Applications in the natural environment include the evolution of ribbed scales in sharks (Fletcher et al., 2014), and the formation of bed forms, such as dunes, in sediment carrying flows (Best, 2005). Previous work of Arfaie et al. (Arfaie et al., 2014; Arfaie, 2015) has shown that there are optimal patterns of large-scale roughness elements, such as ribs, to maximise turbulence or to minimize flow resistance. This conclusion apparently supported the work of Eggenhuisen and McCaffrey (2012), who proposed that run-out lengths of particulate gravity currents are enhanced by the presence of rugose bed forms on the ocean floor, such as scours and dunes. Eggenhuisen and McCaffrey conducted gravity current experiments where the flow was perturbed by the presence of a single rectangular roughness element. They observed that the profiles for vertical turbulent normal stresses showed enhanced mixing compared to unperturbed turbulence profiles and concluded that enhanced mixing via bed forms result in a net distribution of sediments towards the upper region of the flow, and thus a reduction in density stratification and an increase in the run-out distance of the flow.

Turbidity current run-out length is controlled by the balance of potential to kinetic energy conversion as a function of the rate of energy dissipation through drag, diffusion and viscous dissipation. The potential energy is controlled by the balance of turbulent particle diffusion with gravitational settling. Thus maximizing flow turbulence is expected to increase the eddy diffusivity of particles, the potential energy of the flow and hence promote greater run out (Eggenhuisen et al., 2010, 2011; Straub et al., 2011; Tokyay et al., 2011).

Arfaie et al. (2014) sought to find further support for this hypothesis by performing a series of numerical investigations to study the effect of lower boundary roughness on turbulent flow in a two-dimensional channel. Periodic arrays of rectangular roughness elements were considered over a wide range of roughness spacing to height ratios, w/k. Computations of volume averaged eddy viscosity were performed over this range in order to establish the optimum spacing that produces maximum turbulence enhancement and mixing. This was found to

* Corresponding author.
E-mail address: a.d.burns@leeds.ac.uk (A.D. Burns).

https://doi.org/10.1016/j.envsoft.2018.06.002
Received 5 December 2017; Received in revised form 19 April 2018; Accepted 1 June 2018
Available online 15 June 2018
1364-8152/

occur when w/k is approximately equal to 7. Moreover, this value is only weakly dependent on Reynolds number, and the decay rate of turbulence enhancement as a function of w/k beyond the optimum spacing is slow. In addition to this, computations of friction factor as a function of w/k indicated that maximum resistance to flow also occurs at the same value of $w/k = 7$. Consequently, the implications on particulate gravity current run-out length were inconclusive, as optimized turbulence mixing tends to act to keep particles in suspension, hence increasing run-out length, whilst optimized resistance acts as a large drain on turbulence kinetic energy, hence decreasing run-out length.

The purpose of this paper is to extend the work of Arfaie et al. (2014) to consider the flow over idealized bed form shapes encountered in geophysical flows, such as dunes, anti-dunes, and symmetric triangular bed forms. This builds on work by McLean et al. (1999) who constructed semi-analytical models based on boundary layer theory for velocity profiles, and boundary shear stresses for flows over two-dimensional dunes. They emphasized the importance of splitting the total drag force on the bed into the pressure drag, or form drag, and the viscous drag, or skin friction. The former is largely responsible for draining the flow of mean kinetic energy, whilst the latter is largely responsible for erosion of particles from the bed into suspension, hence increasing potential energy. Subsequent developments are reviewed by Best (2005) in the context of dunes in rivers. Furthermore, similar CFD research has been carried out to model air flows and sediment transport over aeolian dunes (Feng and Ning, 2010; Parsons et al., 2004; Takahashi et al., 1998; Wakes et al., 2010) and air pollution dispersion over urban canyons (Yang and Shao, 2008; Solazzo et al., 2009; Chu et al., 2005). We perform computational fluid dynamics (CFD) calculations to obtain detailed information on the flow over a variety of idealized two-dimensional dunes. The results are then used to obtain information on the resistive drag and turbulence mixing characteristics as a function of dune shapes and aspect ratios, with particular emphasis on the correlation between flow resistance and turbulent mixing for the different shapes.

In addition to the environmental flow applications considered here, dunes deposited from suspended particles have a significant effect on the flow resistance and sediment carrying capacity of engineering conduits and pipelines, such as those employed in sewage systems (May 1993; Skipworth et al., 1999; Coleman et al., 2003). May 1993 reported on experimental results and models for the effects of a wide range of dune types deposited by non-cohesive particles in sewage systems, noting that their effects were indeed significant, as minimum slope and flow velocities need to be specified in order for sewers to become self-cleansing. This work was extended to cohesive particles by Skipworth et al. (1999). Coleman et al. (2003) performed experiments that indicated that dunes deposited in closed conduits have much in common with dunes formed under free surface flows.

2. Methods

2.1. Numerical method

Simulated flow over complex bedforms was modelled using the numerical method employed by Arfaie et al. (2014). Further details may be found in the PhD thesis of Arfaie (2015). Arfaie et al. used a commercial CFD code ANSYS CFX-14.0 (ANSYS CFX, 2011) to compare the predictions of a wide range of Reynolds Averaged Navier-Stokes (RANS) based turbulence models with the experimental results of Djenidi et al. (1999) and the numerical Large Eddy Simulations of Cui et al. (2003). The standard k-ε model (Launder and Spalding, 1974), used herein, was found to give adequate predictions of flow velocity profiles, and to provide the best compromise between accuracy and computational efficiency in order to permit the exploration of a wide parameter space.

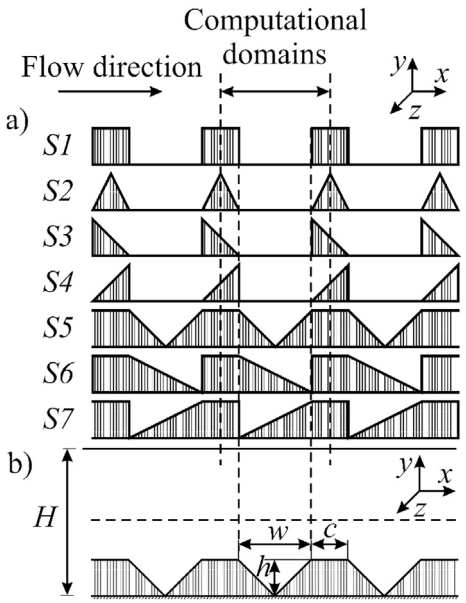

Fig. 1. (a) Schematic illustration of the computational domains shown by the dashed lines for pressure driven flow over idealized bedforms under a periodic condition. (b) Channel flow configuration with roughness segment S5 positioned at the solid bed.

2.2. Idealized bedforms

The rib roughness elements studied by Arfaie et al. (2014) are generalised to idealized shapes, similar to those studied by Moon et al. (2014). The shapes considered here are intended to represent bed forms occurring in the natural environment, see Fig. 1. The shapes $S1$ are the rectangular roughness elements considered by Arfaie et al. (2014). Shapes $S2 - S4$ represent symmetric bed forms, anti-dunes and dunes respectively. Shapes $S5 - S7$ combine the simple shapes $S1 - S4$ to approximate more realistic natural lower boundary rugosities of symmetric dunes, anti-dunes and normal dunes, respectively. Arfaie et al. (2014) employ the categorisation of Perry et al. (1969) of roughness elements into two distinct types of roughness, namely, $d - type$ and $k - type$, where d and k denote channel height and roughness height, respectively. For a sufficiently low width-to-height ratio, $w/k \lesssim 2$, the flow undergoes a skimming flow regime, in which there is little interaction from the vicinity of the roughness element to the outer flow region. This is known as $d - type$ roughness. The $k - type$ roughness regime is associated with $w/k \gtrsim 4$, where the flow in the roughness cavity begins to interact with the main body of the flow. See Jimenez (2004) for a detailed discussion of $d - type$ and $k - type$ roughness regimes. Here, the roughness element height is denoted by h, and we perform a study of the effect of axial roughness length to height ratio (c/h). The upper flat surface length of the roughness element c is varied while the roughness element height is held fixed to cover aspect ratios $c/h = 1$, 2,4 and 8 for each of the bed geometries. The width-to-height ratio w/h is kept fixed at the value $w/h = 7$ which was determined by Arfaie et al. (2014) to give optimal turbulent mixing and flow resistance for rectangular roughness elements. We have not established that this is optimal for all the shapes considered here; it is kept fixed in order to reduce the number of simulations that need to be performed.

2.3. Model assumptions

A shear flow of pure seawater over the idealized bed forms is considered. It is assumed that the particle concentrations are sufficiently small that they do not have a significant influence on the flow field. There is strong evidence that this configuration also gives insight into behavior of dilute sediment gravity flows over bed forms; the velocity

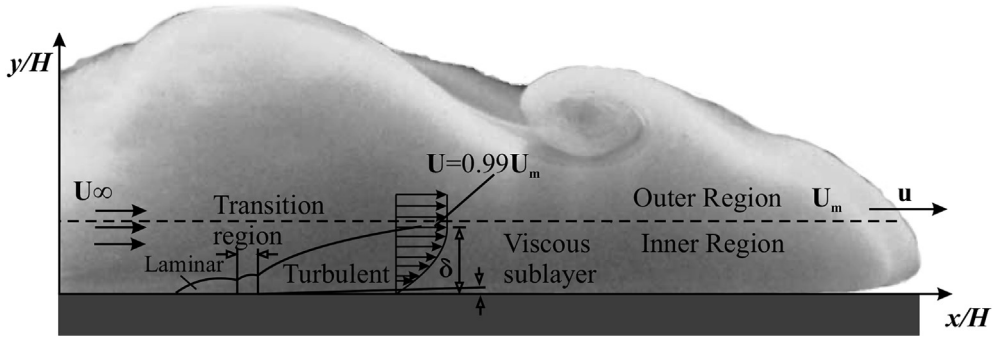

Fig. 2. The structure of turbidity currents modified from the work by Kneller et al. (Kneller et al., 1999) and Simpson (Simpson, 1972). Note: the velocity profile below the velocity maximum approximates that of a shear flow.

profiles of such flows in the inner wall region (below peak velocity) resemble those in fully developed channel flows (Kneller et al. (1999), Eggenhuisen and McCaffrey (2012), Fig. 2).

Numerical simulations were conducted for fully-developed turbulent flow over a range of idealized bed forms, see Fig. 1. The flow field was assumed to be periodically repetitive in the stream-wise direction. Consequently, the computational domain was restricted to describe the flow over a single roughness element, as shown in Fig. 1 (a). The lower boundary was comprised of a hydraulically rough bed of one of forms $S1 - S7$, whilst the upper boundary was flat, with no-slip boundary conditions imposed on both upper and lower boundaries. The flow was driven by applying a constant mean pressure gradient $\overline{\partial p/\partial x}$ added as a source term in the x-momentum equation. The derived periodic pressure field therefore represents fluctuations about a mean pressure field which is linear in the x-direction. The flow was of density $\rho = 1027\,\mathrm{kgm}^{-3}$ and kinematic viscosity $\nu = 1.36 \times 10^{-6}\mathrm{m}^2\mathrm{s}^{-1}$, typical of seawater. A value of $\overline{\partial p/\partial x} = 0.5\,\mathrm{kg\ m}^2\mathrm{s}^2$ was chosen to achieve a high friction shear Reynolds number $Re_\tau \approx 10^5$, where $Re_\tau = (u_\tau H/2)\nu$ is based on the shear velocity $u_\tau = \sqrt{H/(\rho(\overline{\partial p/\partial x})}$ and half-channel height $H/2$. This was motivated by the findings of Arfaie et al. (2014) that turbulent flow over rugose bed forms is only weakly dependent upon Reynolds number.

3. Results and discussion

3.1. Velocity fields

Here we analyze how the various idealized bed form shapes modulate the flow velocity field. Velocity magnitude contours are plotted as a function of bed form topography and aspect ratio. Shapes 1–4 in Fig. 3 behave as $k - type$ roughness elements as the cavity length w is larger than the height h, $(w/h = 7)$. The $d - type$ surfaces $(S5 - S7)$ in Fig. 4 are arguably closer to the flat wall case and consequently are less effective at slowing down the flow than the $k - type$ surfaces. Therefore, wall shear stress is greater in $d - type$ bed forms rather than $k - type$ bed forms.

Small secondary recirculating regions are observed behind the downstream edge of shapes $S1 - S4$ and $S7$. The structure of these vortices depends significantly on the fluid-facing slope angle. For example, shapes $S1$ and $S4$ with downstream edges at 90° to the horizontal produce larger vortices compared to shape $S2$, whilst shape $S5$ has no recirculation region at all. Comparison of streamlines for shapes $S3$ and $S6$ indicates that the development of the secondary vortex on the slope facing bed forms does not depend significantly on the spacing between two bed forms. The flow streamlines in Fig. 3 show that, for $k - type$ roughness, the flow separates near the bed form crest, followed by reattachment of the flow on the flat bed next to the adjacent bed forms.

Moreover, the streamlines of shape $S1$ show that as the aspect ratio c/h increases, the focal point of the recirculation region shifts more towards the leading face of the downstream rib, approaching intermediate type roughness behavior. This behavior is also apparent for shape $S4$ where the streamlines become more parallel as aspect ratio values increase from 1 to 8.

3.2. Mean flow and flow resistance

3.2.1. Mean flow

In comparison to a flat bed, the presence of bed forms modulates the flow. Both Figs. 3 and 4 show that as flow obstruction and thus frictional drag is reduced, i.e. as aspect ratio c/h increased, the mean axial flow velocity increases significantly. Also, the re-attachment length increases for all $k - type$ bed forms with the increase in aspect ratio. The behavior in reattachment is attributed to shallowing of the lee slope reducing turbulence intensity and diffusivity in the space between the recirculation region and the next roughness element.

The cross-sectionally averaged stream-wise velocity for flow over bed forms is denoted by U_{rough}. The corresponding quantity for the flat bed case is denoted by U_{flat}, and we use this to normalise the averaged velocity in the rough bed cases. The ratio U_{rough}/U_{flat} is plotted against aspect ratio c/h for all lower roughness boundaries in Fig. 5. Due to obstruction of the flow by bed roughness elements U_{rough}/U_{flat} is strictly less than unity. The maximum average velocity across all aspect ratios is seen for the smoothed roughness element $S5$, reducing flow separation, and the minimum for pointed roughness element $S3$, enhancing flow separation.

Fig. 5 indicates that shape $S2$ has a greater gradient in velocity with respect to change in aspect ratio compared to that of other bed shapes. This result agrees with the DNS results of Orlandi et al. (2016) in which a higher average flow velocity is seen over triangular bars compared to square bars. In addition, there is an increase in velocity between the $d - type$ and the $k - type$ flows. However, the magnitude of this shift decreases with the increase in aspect ratio. The value of U_{rough}/U_{flat} in the idealized asymmetric dune $S4$ is greater than that of the idealized symmetric dune $S2$.

3.2.2. Flow resistance

As all simulations are performed under a fixed imposed pressure gradient, the results described above on variation of mean velocity with shape and aspect ratio are a consequence of the variation of resistance to flow as these quantities are varied. The resistance to flow over the various bed geometries is computed using the Darcy-Weisbach friction factor f defined in equation (1), based on the specified mean pressure gradient $\partial p/\partial x$ and the averaged stream velocity $\overline{U}$

$$f = \frac{(H/2)(-\partial p/\partial x)}{0.5\rho\overline{U}^2} \tag{1}$$

Fig. 6 plots friction factor against aspect ratio of each of the bed form shapes. The results show that the friction factor decreases with increasing aspect ratio for all bed form shapes. The maximum flow

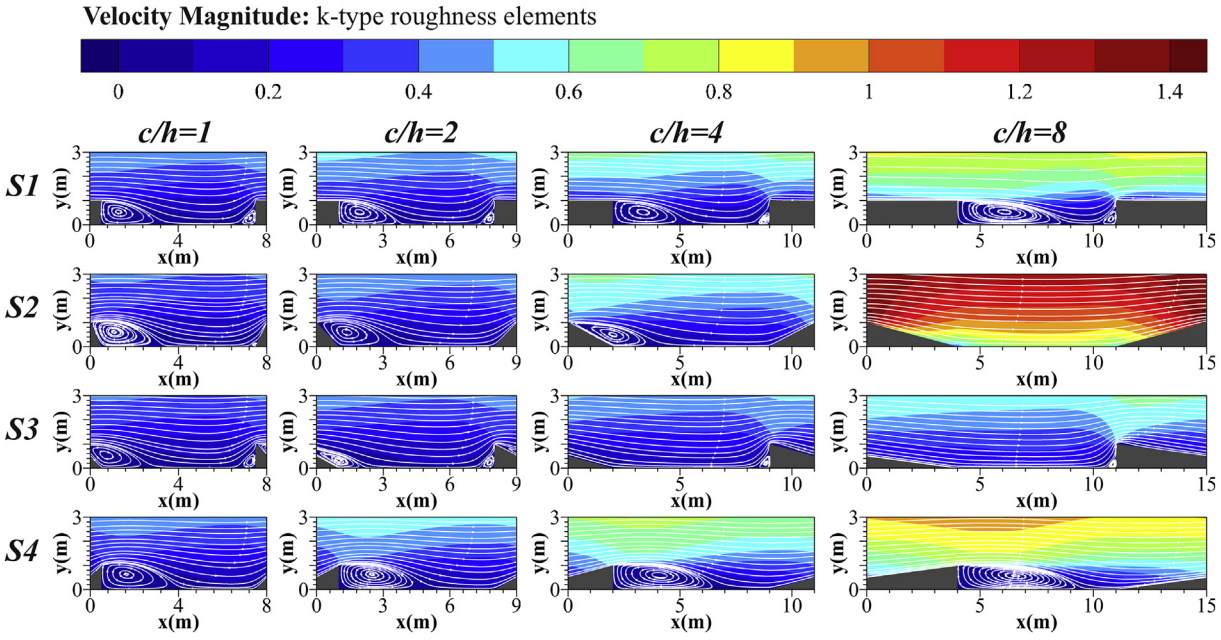

Fig. 3. Matrix view of the velocity magnitudes with flow streamlines over *k*-type bed forms with varying aspect ratio c/h.

resistance occurs for the transport of fluid over shape $S3$ and the minimum flow resistance occurs for shape $S5$. The friction factor is greater for $k-type$ (with spacing) roughness elements than $d-type$ (without spacing) cases.

3.2.3. Skin friction and form drag

In order to understand the dynamics of natural flows over bed forms, it is necessary to partition the total shear stress at the bottom boundary into the separate components of skin friction and form drag (McLean et al., 1999). The skin friction is the component due to tangential stresses (viscous forces), and this is a determining factor for the rate of entrainment of sediment from the bed into the main flow. The form drag is the component due to normal stresses (pressure forces). For flow over blunt roughness elements, this is usually the dominant contributor to the overall drag force, due to flow separation generating large differences in pressure between the front and the back of the element.

The skin friction and form drag are determined by integrating the viscous and pressure forces along the wall, as described in equations (2)

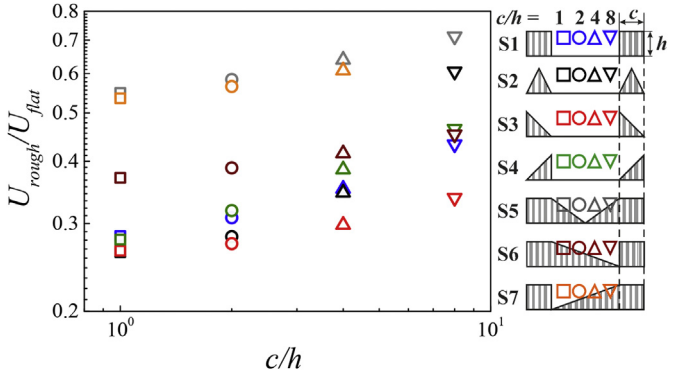

Fig. 5. Normalized stream-wise mean velocity as a function of aspect ratio for all bed roughness cases.

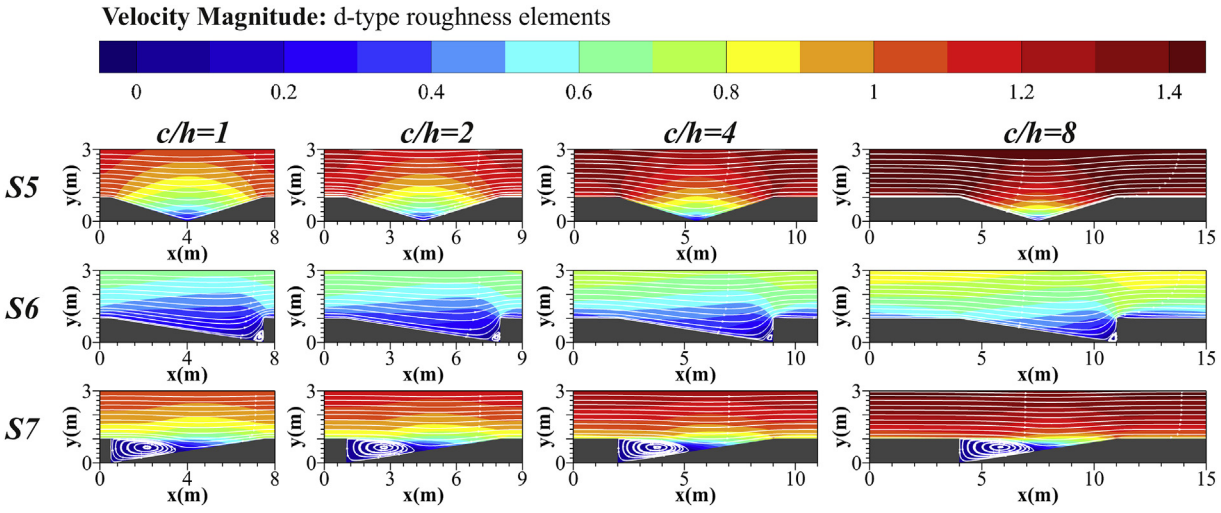

Fig. 4. Matrix view of the velocity magnitudes with flow streamlines over *d*-type bed forms with varying aspect ratio c/h.

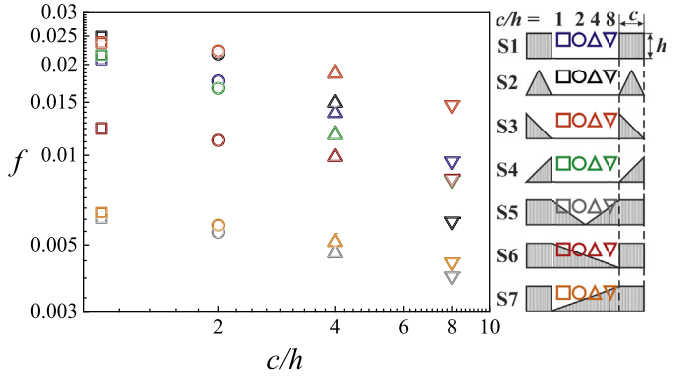

Fig. 6. Darcy-Weisbach friction factor as a function of aspect ratio for flows over different roughness elements.

and (3) respectively

$$\overrightarrow{F_v} = \int_w \tau_w \vec{s} \,.\, \vec{x}\, ds \tag{2}$$

$$\overrightarrow{F_p} = \int_w p\vec{n} \,.\, \vec{x}\, ds \tag{3}$$

The relative change in the skin friction and form drag are determined by non-dimensionalising the friction components (2) and (3) with the force applied to the lower boundary,

$$D_s = \frac{|\overrightarrow{F_v}|}{1/2\rho u_f^2 A_w} \tag{4}$$

$$D_f = \frac{|\overrightarrow{F_p}|}{1/2\rho u_f^2 A_p} \tag{5}$$

Here u_f is the area-weighted average velocity u of the fully developed flow at the outlet of the flat bed case. The skin friction (4) employs the wetted areas A_w, which for aspect ratios c/h = 1,2,4,8 are given by A_w = 9,11,15,23 m^2 respectively. The form drag (eqn. (5)) employs the projected area A_p, which is equal to 1 m^2 for all bedform simulations.

Fig. 7 plots absolute values of the form drag against skin friction for all bed form shapes and aspect ratios. Both skin friction and form drag are found to increase with increase in aspect ratio for all bed form shapes. The increase is due to the integral of the pressure and viscous forces for the extended surface produced by the increase in aspect ratio c/h. Further, Fig. 7 indicates that the value of skin friction is greater for $d-type$ than for $k-type$ bed forms. This is primarily due to either the lack of flow separation ($S5$ and $S6$), or flow separation with reattachment on the downstream sloped edge next adjacent element ($S7$) leading to a low pressure gradient. Consequently the value of form drag is greater for the $k-type$ than the $d-type$ bed forms.

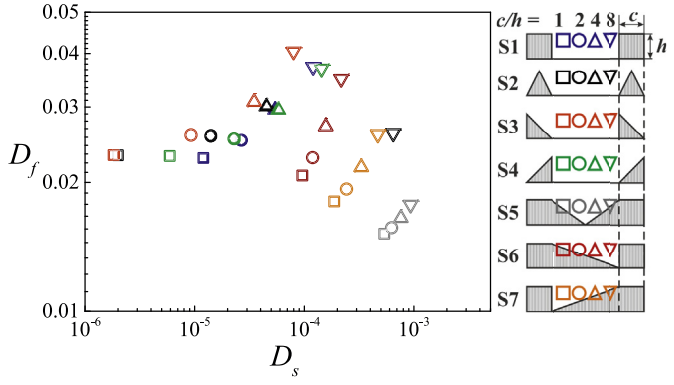

Fig. 7. Form drag versus skin friction for all bed forms and aspect ratios.

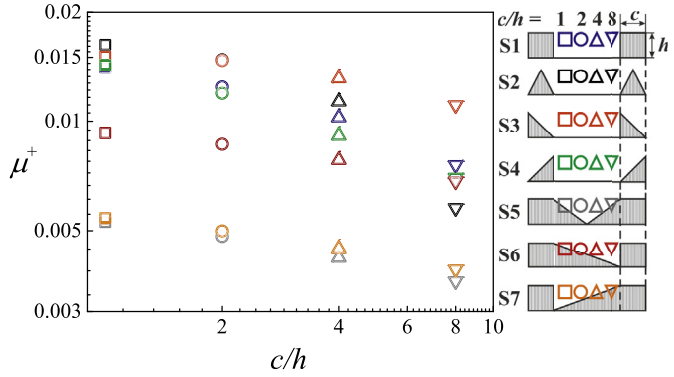

Fig. 8. Normalized eddy viscosity as a function of aspect ratio c/h.

3.3. Turbulent mixing

Arfaie et al. (2014) measured the amount of turbulent mixing in a periodically rectangular rib roughened channel using the non-dimensionalised eddy viscosity μ^+,

$$\mu^+ = \frac{\mu_t}{\rho \overline{U}\,(H/2)} \tag{6}$$

Here we use μ^+ to evaluate the turbulent mixing potential of different bed geometries. Fig. 8 plots the average value of μ^+ as a function of c/h for all bed geometries. The overall results suggest that bedforms with high flow resistance also result in high turbulent mixing. The data further shows that μ^+ is reduced as the aspect ratio of the bed forms is increased. The lowest turbulent mixing occurs for bed form shapes with closed spacing ($S5-S7$) and the highest for bed forms ($S1-S4$). The comparison of Figs. 7 and 8 suggests that turbulent mixing depends more on form drag than skin friction.

An important conclusion that can be made is that the strong correlation between turbulent mixing and flow resistance found by Arfaie et al. (2014) for rectangular bedforms is also seen for the full range of bed form shapes considered here. Fig. 9 plots the non-dimensionalised measures of flow resistance (friction factor f) and turbulence mixing (normalized eddy viscosity μ^+) against each other for all bedform shapes and aspect ratios considered here. Significantly, the data effectively collapse onto the same straight line for all bed form shapes. This result is reminiscent of the observation that the friction factor for turbulent flow in a rough conduit correlates well with flow Reynolds number and roughness height, but is apparently independent of roughness morphology at least up to 5% relative roughness (Taylor et al., 2006). Fig. 9 indicates that this degree of universality may extend to the larger roughness elements considered here.

Shape $S5$ produces the least flow resistance and mixing. The low

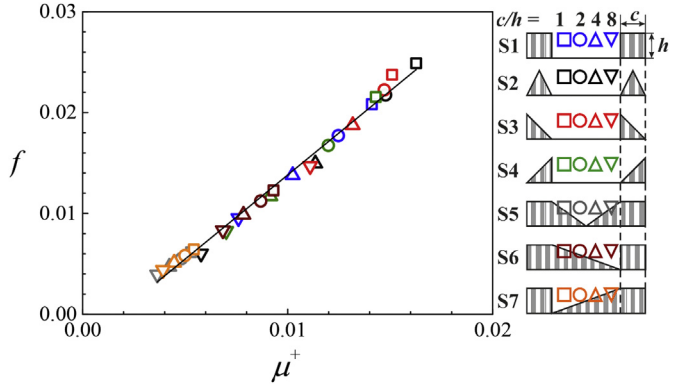

Fig. 9. Friction factor as a function of normalized eddy viscosity for all bedforms.

value of vertical mixing in this case appears to be caused by the lack of flow separation and the closed gap between two adjacent bed forms. Moreover, the results indicate that flow separation has an insignificant effect on the value of upward sediment mixing for the skimming flow type ($S5 - S7$), where the flow reattaches on the slope of the downstream roughness element. Fig. 9 further illustrates that the blunt facing bed forms $S5$ and $S7$ achieve a higher turbulent mixing than the slope facing bed form $S6$. $k - type$ surfaces also show an increase in μ^+ and f with the orientation of the downstream facing flow (or stoss side). For instance, shapes $S2$ and $S4$ lead to reductions in the values of mixing and flow resistance compared to shape $S1$ and $S2$ (with 90° side facing flow angle). For the $k - type$ surfaces the effect of flow separation on the flow resistance and turbulent mixing is also weak. This effect is described for shape $S3$ at $c/h = 2$ (with flow separation) and $c/h = 4$ (with absence of flow separation) in Fig. 3.

3.4. Discussion

The rate of sediment entrainment is a function of the skin friction. Therefore Fig. 7 predicts that the sediment entrainment rate is greater for bed forms $S5 - S7$ ($d - type$) than for $S1 - S4$. The results also predict that the suspension of the sediment should be greater for $k - type$ than for $d - type$ surfaces. Both the sediment suspension and entrainment rate are predicted to increase with the decrease in slope angle.

Finally, in accord with the results of Arfaie et al. (2014) we cannot conclude that any of the shapes considered definitively promote or reduce run out length, due to the subtle interplay that occurs between the competing effects of flow resistance and turbulent mixing on the overall kinetic and potential energy budgets.

Note that this work has considered integrally averaged measures of flow resistance and turbulent mixing for flows of pure liquid, neglecting details of particle transport. The results suggest that, in order to elucidate further the effects of bed form roughness on the energy budget of sediment-bearing flows, such as turbidity currents, further work is needed that investigates the details of particle concentrations, sedimentation and flow capacity. This will be the subject of further investigations.

4. Conclusions

Numerical simulations have been performed at a high Reynolds number for shear flow over a series of lower boundary roughness elements comprising a range of idealized bed form shapes, of varying crestal length to height ratio c/h at a fixed width to height ratio (w/h). The total basal shear stress is split into skin friction and form drag, with sediment entrainment proportional to skin-friction and turbulent mixing proportional to the sum of skin friction and form drag. Here we show how the respective magnitudes of these friction components vary as a function of scale of various bed form roughness shapes, with both $d - type$ and $k - type$ characteristics. Sediment erosion is expected to be greatest in the $d - type$ bed forms where skin friction is observed to be largest. The results also demonstrate how bed forms affect the balance of energy lost (through frictional effects) as a function of the potential energy gained (through turbulent mixing).

The results indicate that, for all bed form shapes considered, both the friction factor and the dimensionless eddy viscosity decrease with increasing aspect ratio. Thus, flow resistance and turbulent mixing are strongly correlated, with maximum resistance coinciding with maximum mixing for all shapes considered. Fig. 9 indicates that the relation between flow resistance to eddy viscosity collapses to a single monotonically increasing linear function for all bed forms considered. This result is significant, as it supports the conjecture that the relations between frictional and mixing characteristics of the flows that we have considered are independent of the detailed morphology of the individual roughness elements.

Software availability

SoftwareANSYS-CFX
Programming languagesFortran 90/77 and CEL
Discretization techniqueFinite volume
Current version14.0
AvailabilityDownload definition file from https://Ωdrive.google.com/drive/folders/1XHNEXllzCivBDtAMycox1QRV–d_ΩBB5D?uspsharing
Operating systemLinux and Windows
LicenseCommercial
HPCDual socket with quad-core Intel X5560 (2.8GHz) processors per server; 12GB of DDR3 1333MHz memory per server, 24GB flash disk and QDR Connect-X infiniband (ARC1 University of Leeds).
Parallel Run ModeMPI (8 nodes and 8 processes per node used)
Contact addressANSYS UK Ltd, Abingdon, United Kingdom
Telephone + 44 (0) 800 048 0462
FaxNone
Emailsupport-uk@ansys.com
Web pagehttps://www.ansys.com
Year First available1991
Plotting toolTecplot, https://www.tecplot.com/

Acknowledgements

This research was funded by the Turbidites Research Group industry consortium (2011-2013 Phase: Anadarko, BG, BHP Billiton, BP, ConocoPhillips, Maersk, Marathon, Nexen, Statoil, Tullow and Woodside.)

Appendix A. Supplementary data

Supplementary data related to this article can be found at http://dx.doi.org/10.1016/j.envsoft.2018.06.002.

References

ANSYS CFX, 2011. Theory Guide, vol. 14 Ansys Inc.
Arfaie, A., 2015. Numerical Modelling of the Influence of Lower Boundary Roughness on Turbulent Sedimentary Flows. Ph.D. thesis. University of Leeds.
Arfaie, A., Burns, A., Dorrell, R., Eggenhuisen, J., Ingham, D., McCaffrey, W., 2014. Optimised mixing and flow resistance during shear flow over a rib roughened boundary. Int. Commun. Heat Mass Tran. 58, 54–62.
Best, J., 2005. The fluid dynamics of river dunes: a review and some future research directions. J. Geophys. Res.: Earth Surface 110.
Chu, A., Kwok, R.C.-W., Yu, K., 2005. Study of pollution dispersion in urban areas using computational fluid dynamics (cfd) and geographic information system (gis). Environ. Model. Software 20, 273–277.
Coleman, S.E., Fedele, J.J., García, M.H., 2003. Closed-conduit bed-form initiation and development. J. Hydraul. Eng. 129, 956–965.
Cui, J., Patel, V.C., Lin, C.-L., 2003. Large-eddy simulation of turbulent flow in a channel with rib roughness. Int. J. Heat Fluid Flow 24, 372–388.
Djenidi, L., Elavarasan, R., Antonia, R., 1999. The turbulent boundary layer over transverse square cavities. J. Fluid Mech. 395, 271–294.
Eggenhuisen, J.T., McCaffrey, W.D., 2012. The vertical turbulence structure of experimental turbidity currents encountering basal obstructions: implications for vertical suspended sediment distribution in non-equilibrium currents. Sedimentology 59, 1101–1120.
Eggenhuisen, J.T., McCaffrey, W.D., Haughton, P.D., Butler, R.W., 2010. Small-scale spatial variability in turbidity-current flow controlled by roughness resulting from substrate erosion: field evidence for a feedback mechanism. J. Sediment. Res. 80, 129–136.
Eggenhuisen, J.T., McCaffrey, W.D., Haughton, P.D., Butler, R.W., 2011. Shallow erosion beneath turbidity currents and its impact on the architectural development of turbidite sheet systems. Sedimentology 58, 936–959.
Feng, S., Ning, H., 2010. Computational simulations of blown sand fluxes over the surfaces of complex microtopography. Environ. Model. Software 25, 362–367.
Fletcher, T., Altringham, J., Peakall, J., Wignall, P., Dorrell, R., 2014. Hydrodynamics of fossil fishes. In: Proc. R. Soc. B, vol. 281. The Royal Society, pp. 20140703.
Jimenez, J., 2004. Turbulent flows over rough walls. Annu. Rev. Fluid Mech. 36, 173–196.
Kim, H.-M., Kim, K.-Y., 2006. Shape optimization of three-dimensional channel roughened by angled ribs with rans analysis of turbulent heat transfer. Int. J. Heat Mass Tran. 49, 4013–4022.

Kneller, B.C., Bennett, S.J., McCaffrey, W.D., 1999. Velocity structure, turbulence and fluid stresses in experimental gravity currents. J. Geophys. Res.: Oceans 104, 5381–5391.
Launder, B.E., Spalding, D.B., 1974. The numerical computation of turbulent flows. Comput. Meth. Appl. Mech. Eng. 3, 269–289.
May, R., 1993. Sediment Transport in Pipes, Sewers and Deposited Beds. Technical Report, HR Wallingford. .
McLean, S., Wolfe, S., Nelson, J., 1999. Spatially averaged flow over a wavy boundary revisited. J. Geophys. Res.: Oceans 104, 15743–15753.
Moon, M.-A., Park, M.-J., Kim, K.-Y., 2014. Evaluation of heat transfer performances of various rib shapes. Int. J. Heat Mass Tran. 71, 275–284.
Orlandi, P., Sassun, D., Leonardi, S., 2016. Dns of conjugate heat transfer in presence of rough surfaces. Int. J. Heat Mass Tran. 100, 250–266.
Parsons, D.R., Wiggs, G.F., Walker, I.J., Ferguson, R.I., Garvey, B.G., 2004. Numerical modelling of airflow over an idealised transverse dune. Environ. Model. Software 19, 153–162.
Perry, A.E., Schofield, W.H., Joubert, P.N., 1969. Rough wall turbulent boundary layers. J. Fluid Mech. 37, 383–413.
Simpson, J.E., 1972. Effects of the lower boundary on the head of a gravity current. J. Fluid Mech. 53, 759768.
Skipworth, P.J., Tait, S.J., Saul, A.J., 1999. Erosion of sediment beds in sewers: model development. J. Environ. Eng. 125, 566–573.
Solazzo, E., Cai, X., Vardoulakis, S., 2009. Improved parameterisation for the numerical modelling of air pollution within an urban street canyon. Environ. Model. Software 24, 381–388.
Straub, K.M., Mohrig, D., Buttles, J., McElroy, B., Pirmez, C., 2011. Quantifying the influence of channel sinuosity on the depositional mechanics of channelized turbidity currents: a laboratory study. Mar. Petrol. Geol. 28, 744–760.
Takahashi, S., Du, M., Wu, P., Maki, T., Kawashima, S., 1998. Three dimensional numerical simulation of the flow over complex terrain with windbreak hedge. Environ. Model. Software 13, 257–265.
Taylor, J.B., Carrano, A.L., Kandlikar, S.G., 2006. Characterization of the effect of surface roughness and texture on fluid flowpast, present, and future. Int. J. Therm. Sci. 45, 962–968.
Tokyay, T., Constantinescu, G., Meiburg, E., 2011. Lock-exchange gravity currents with a high volume of release propagating over a periodic array of obstacles. J. Fluid Mech. 672, 570–605.
Wakes, S.J., Maegli, T., Dickinson, K.J., Hilton, M.J., 2010. Numerical modelling of wind flow over a complex topography. Environ. Model. Software 25, 237–247.
Webb, R., Eckert, E., 1972. Application of rough surfaces to heat exchanger design. Int. J. Heat Mass Tran. 15, 1647–1658.
Yang, Y., Shao, Y., 2008. Numerical simulations of flow and pollution dispersion in urban atmospheric boundary layers. Environ. Model. Software 23, 906–921.